

Comparative study of Raman modes active, emission bands and thermal features of GS α - Al_2O_3 NP's

H. A. T. Al-Ogaili ^{*a}, N. J. Jubier ^b, A. A. Thamer ^c

^{a,b,c}*Department of Physics, college of science, Wasit University, Wasit, Iraq*

This work, focuses on spectroscopic features such as PL and Raman and thermal analysis such (TGA –DSC) for the nanoparticles of aluminium oxide (GS α - Al_2O_3) synthesizes by two plant solutions (leaves (S1) and phloem(S2)) at room temperature. In different reactions, plant extracts are mixed with metal precursor solutions, Various reactions are carried out with metal precursor solutions when plant extracts are combined with them and biomolecules are responsible for reducing metal ions and capping the bio-reduced metal nanoparticles synthesized by using plant extract. As a result, calcination of the products of powder alumina at 1800°C found that the phase was α - Al_2O_3 , analysis of PL was achieved when excited of two samples (S1 and S2) by different wavelengths at 200 nm,250nm and 300 nm, it gave at $\lambda_{\text{ex}}=300\text{nm}$, three peaks of emission at 295 nm, 350 nm 590 for S1 and 300 nm 360 nm 590nm for S2 respectively at the E_g values 4.2,2.9,2.1eV and 4.1eV and 3.4,2.1eV from UV to the yellow range, results in thermal analysis notice that rapidly loss in the weight to reach for the stable phase of α - Al_2O_3 . Raman active modes have seven actives for both prepared samples S1 and S2, these samples of Al_2O_3 can be applied in high-performance heat and dye degradation.

(Received December 8, 2024, Accepted March 31, 2025)

Keywords: α - Al_2O_3 , PL, TGA-DSC, Raman mode, Green route

1. Introduction

Extensive research has been conducted on numerous inorganic metal oxides as nanostructures, including insulators (Al_2O_3), semiconductors with broadband gaps (ZnO), and transition metal oxides (NiO), both doped and pure. The wide range of applications and fascinating properties of these oxides have led to extensive research activities [1-3]. Al_2O_3 exhibits various transition polymorphs at different temperatures, including face-centred-cubic, monoclinic, orthorhombic, hexagonal close-packed, and thermodynamically stable α - Al_2O_3 (corundum) structures [4-6]

Recently, metal oxides have been explored as possible Nanofluids for high-performance heat/energy exchange technologies [7]. Materials with nanoscale structures have different thermal characteristics, Scientists and engineers have observed a sharp increase in interest in oxide nanoparticles' capacity to conduct heat [8]. Thermal properties are essentially focused on how a material responds to the application of heat, examples of these properties include heat capacity (atomic vibrations, phonons, and electron contribution), thermal expansion, thermal stresses, thermal diffusivity (α), thermal effusivity (e), and thermal conductivity (k ; rate of heat transfer through a material by electrons and phonons). With the ever-growing demand and increased operating speed, there has been a great deal of attention on increasing the efficiency of heat exchange systems by nanoparticle additives [9] Nanotechnology has led to miniaturization, requiring new materials and methods, for example in the field of thermal convection fluids, innovative and excellent cooling concepts have been developed. Additionally, metal oxide nanostructures can exhibit striking photoluminescence properties, making them a key component of many optoelectronic devices. Nanomaterials undergo optical transitions when a photon is absorbed or emitted by defects at their surface, as optical transitions in nanomaterials are generated by absorbing or emitting photons due to the presence of relevant defects at the oxide surface [10]. The large band

* Corresponding author: halukely@uowasit.edu.iq
<https://doi.org/10.15251/DJNB.2025.201.365>

gap material has a wider separation of energy as a result This difference is called the conduction band-valence band gap, and it's important for good transparency of materials [11] Oxides with nanometer-scale properties have caught the attention of many electronic device components [12]. Oxides with nanometer-scale properties have caught the attention of many electronic device components based on their phases. through the design of metal oxide nanomaterials and their analysis, it was found that surface effects are important in designing structural properties which their phase-dependent [13-14]

Considering the structural properties is important because metal oxide nanostructures are available in both crystalline and amorphous forms, determining their activity and selectivity in various applications.

A fraction of uncontrolled impurities can cause photoluminescence in nominally pure aluminium oxide nanopowders. Metal oxides are more readily synthesized and more stable than aluminium oxides. Luminescence of impurity centers was observed in Al_2O_3 Nano powders. Transition metals Fe, Ti, and Cr are usually the uncontrolled impurities that affect the luminescence properties of alumina, which can all contribute to its long wavelength emission. When the aluminium oxide lattice is calcined at high temperatures, a phase transition occurs due to the change in crystal field symmetry that affects electron transition probability in impurity centres. Considering the presence of the 320 nm band in the excitation spectra of prepared samples belonging to phase α and phase γ , an assumption has been made regarding the significance of hydroxyl group centres on the surface [15].

Increasingly, green synthesis is becoming popular because it is environmentally safe, commercially scalable, versatile, cost-effective, simple and efficient on a large scale. The study used two plant extracts to synthesize Al_2O_3 nanoparticles.

Currently, it has been prepared the phase of α - aluminium oxide via biosynthesis with high stability and ease of synthesis and has been discussed the results of the spectroscopic and thermal

2. Biosynthesis of α - Al_2O_3 NP

Manufacturing Al_2O_3 (NPs) using leaves of Laure (S1) *Cinnamomum verum* (phloem S2) and extracts to aluminium nitrate solutions involves several steps. Firstly, the raw materials are mixed and stirred in a beaker until they form a homogeneous solution. Secondly, the solution is heated to a temperature of 60°C for about 30 minutes to allow the desired reaction to occur [16,17]. Thirdly, the solution is cooled to room temperature before filtering it to obtain the Al_2O_3 NP precipitate. Finally, the precipitation is milled to obtain a greenish-white or brown-white powder as desired and calcination at 1800°C .

This work focuses on the efficient and fast green synthesis(GS) of Al_2O_3 -NPs using *Cinnamomum verum* and Laurel leaf extracts. The process begins with the extraction of leaves, followed by the addition of an aqueous solution of aluminium nitrate. It was observed that the mixture yielded greenish-white and brown-white precipitates within a span of 6-10 minutes. The Al_2O_3 -NPs obtained were then subjected to PL, Raman and Thermal analyses to ascertain their primary and secondary size and shape.

3. Results and discussion

3.1. Photoluminescence (PL)

Various kinds of defects emit light in the photoluminescence spectrum according to this study, PL emission depends on the excitation wavelength and is attributed to amorphous carbon or uncontrolled impurities or oxygen vacancies, **Fig 1-S1** shows the PL excitation spectra for α - Al_2O_3 as-formed, this image displays three excitement bands of $\lambda_{\text{ext}} = 200\text{nm}, 250\text{nm}, 300\text{nm}$ for two samples(S1.S2), note that the material of Al_2O_3 excited at $\lambda_{\text{ext}} = 200\text{nm}$, 250 **Fig. 1S1** give two bands only with centres 415,490 nm, so at $\lambda_{\text{ext}} = 250\text{nm}$ the centres at 415, 500 for S1 of Al_2O_3 respectively, in while Fig. 1- S2 illustrates that at $\lambda_{\text{ext}} = 200\text{nm}$, 250 nm give two peaks of each excited with the wavelength where the bands at 420,505,420and 490 nm for S2 of Al_2O_3 , whereas

$\lambda_{\text{ext}}=300\text{nm}$ at 295, 350, 590nm for S1 while peaks 300,360,590 nm for S2 respectively, a notable feature of the first band is its sharpness, while the second and third bands are broader.

It is well-known that the first and second bands at 295 and 350 nm can be attributed to oxygen vacancies in un-doped oxide samples [18,19]. Furthermore, the broadness and peak position (590 nm) of the third band suggest that carbon contained in the samples plays a role [20,21]. It is reasonable to speculate that amorphous carbon is found in the samples because a tiny amount of carbonaceous matter was left behind from the fuel, these emission bands located at UV-and green regions, as a result of a deficiency in Oxygen in the systems due to non-stoichiometry of samples Al_2O_3 that lead to the luminescence of these samples also the element of Al^{+3} as well-known dark and nonluminous, maybe the existence of carbon in samples and increasing C due to enhancement the luminescence [22- 23]

The first emission band at 290,300 nm belong to radiative recombination (band-to-band)[24], the electron occupies the vacancy of oxygen, Specifically, surface hydroxyl groups, known as (^-OHs), are hypothesized to be responsible for this luminescence at 330 nm, assuming they are sensitized by these groups[22] , the second band of emission occurs result from the recombination of the delocalized electron that located near the conducting band[25], the third band emission maybe self- trapped [26], one of the reasons of emissions is the defect levels obtaining of unsaturated bonds and the dangling bonds which existence on the nanostructure of surfaces that supports to form additional levels of energy in the crystals that have a broad bandgap[27].

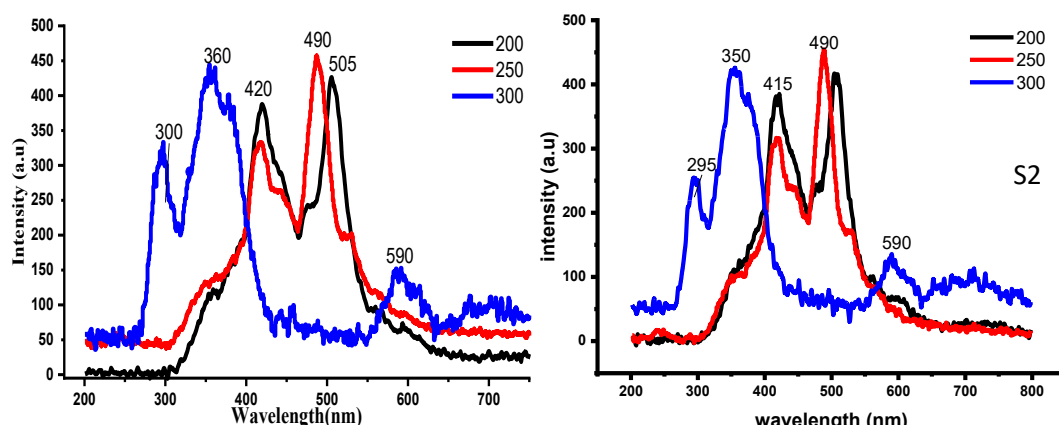


Fig. 1. PL of S1 & S2 GS of $\alpha\text{-Al}_2\text{O}_3$.

3.2. Raman modes

Various materials have been characterized using Raman spectroscopy to analyze their structural attributes, compositions, and phases. Figure 3 shows the Raman spectra of synthesized $\alpha\text{-Al}_2\text{O}_3$ structures for S1 and S2. The $\alpha\text{-Al}_2\text{O}_3$ exhibits seven of the active modes of phonons for Raman modes at the Brillouin zone which gives phonon frequencies at this region. the elastic waves have two modes: one longitudinal optical mode (LO) and two transverse modes (TO), as well-known in $\alpha\text{-Al}_2\text{O}_3$ has optical bands $2A_{1g} + 2A_{1u} + 3A_{2g} + 2A_{2u} + 5E_g + 4E_u$ [28-30] where the terminal ($2A_{1g} + 5E_g$), $A_1(\text{LO})=E_1(\text{LO})$ are Raman active modes, while active modes of IR are $2A_{2u} + 4E_u$, whereas ($2A_{1u}$ and $3A_{2g}$) aren't presented the active modes for Raman and IR. The Raman active modes $173, 249, 335, 428, 606, 810, 868 \text{ cm}^{-1}$ for S1 sample of $\alpha\text{-Al}_2\text{O}_3$, where $A_{1g}=428$ and 810 cm^{-1} $E_g=173, 249, 335, 606, 868 \text{ cm}^{-1}$, whereas $E_g=167, 245, 297, 601, 867 \text{ cm}^{-1}$ 425 and 804 cm^{-1} for S2 sample of $\alpha\text{-Al}_2\text{O}_3$, the results agree with [31], Raman spectroscopy probes the excitation of lower frequencies at 10^{12} Hz (phonons) or lattice relaxation effects in electronic structures while UV-visible measures the excitation of high optical frequencies at 10^{15} Hz [32] Al_2O_3 's electronic structure is governed by several factors at high temperatures such as the interaction between electron and phonon and expansion of thermal lattice

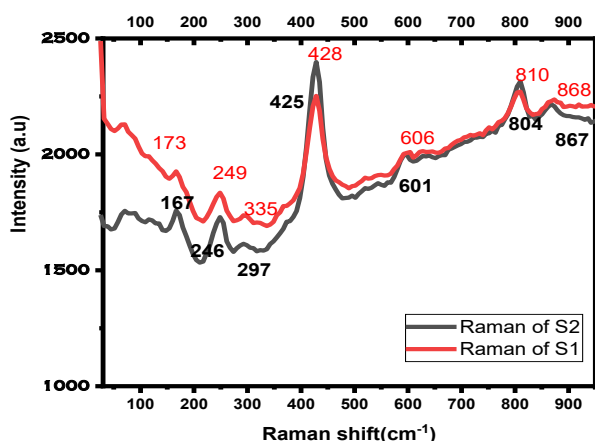


Fig. 2. Raman modes of S1&S2 α - Al_2O_3 .

4. Thermal analysis

To investigate the thermal behaviour of aluminium oxide, thermogravimetric analysis (TGA) was combined with differential scanning calorimetry (DSC), combining these complementary techniques offers valuable insight into the properties of Al_2O_3 samples, including phase transitions, thermal stability, and decomposition. In air, we carried out TG/DSC using a thermal analyzer model along with a temperature increase of $10^\circ\text{C}/\text{min}$, hold for 1.0 min at 40.00°C , Heat from 40.00°C to 600.00°C at $10.00^\circ\text{C}/\text{min}$ S1 sample thermogram indicates that the weight loss up to 250°C is caused by solvents that remain inside the sample after drying and water that has been loosely bound. The thermal stability of the S1 sample is at around 570°C after the initial weight loss is caused by structural rearrangements resulting from phase transformation that result in the loss of OH^- groups.

Fig. 3 A TGA curve indicates a minimal weight loss (0.6%) to 600°C , confirming Al_2O_3 's exceptional thermal stability. A DSC analysis reveals several characteristic features that indicate negligible mass changes below 200°C due to the desorption mainly of water molecules. there is an endothermic peak at approximately 160 - 200°C , associated with the removal of physisorbed water, in relation to the removal of chemisorbed water and surface hydroxyl groups, a broad, shallow endothermic region is present between 300 and 500°C . the materials are studied using TGA to determine their thermal resistance and stability by examining their weight changes with temperature. During the studied temperature range, there were no significant phase transitions, confirming that Al_2O_3 has thermal stability beyond 500°C . The absence of major thermal events in both the TGA and DSC curves Fig.3 and Fig. 4 indicates Al_2O_3 's structural stability at elevated temperatures.

Using TGA and DSC, we found that the Al_2O_3 NPs were thermally stable from 40°C to 200°C . This suggests its suitability for high-temperature applications in solar thermal systems, particularly heat exchangers and heat sinks. During heating, nano-crystalline materials tend to shrink to minimize their energy by reducing the grain boundary area per unit volume, which allows them to store a high amount of energy. Due to their dense grain boundaries, nano-crystalline materials have a high driving force for grain coarsening, which leads to poor thermal stability. In the second stage, the S2 sample exhibits a very similar thermogram to S1 since it contains the same amount of surfactant based on Fig 3. The heat flow as in Fig. 4 has two points of glass transitions for each sample T_g is 164°C , 235.168°C for S1, and 163°C , 236.33°C for S2, respectively.

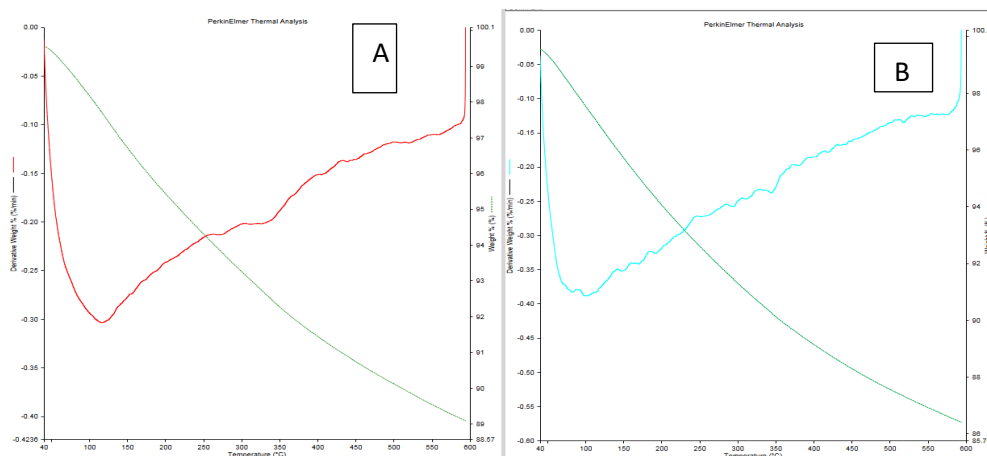


Fig. 3. TGA of α - Al_2O_3 for two samples (A. S1, B- S2).

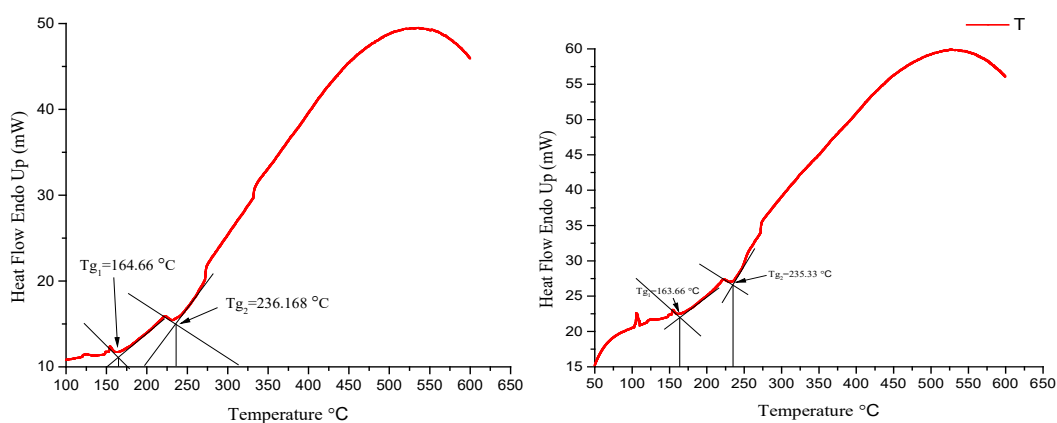


Fig. 6. Heat flow as a function of Temperature for two (S1 & S2).

Then we determined the equation for $-\ln(1-X)$ versus time to determine the reaction rate constants Fig.4 and Fig.5 The plot is linear, confirming first-order kinetics [23]. The value of the rate constant was 0.997 for two samples. An Arrhenius plot, as depicted by the equation $\ln k = -E_a/RT + \ln A$ was used to calculate the activation energy (E_a), $R = 8.314 \text{ J K}^{-1}\text{mol}^{-1}$ and $T = \text{Kelvin}$. For two plants, activation energy (minimize energy for happen reaction) was found to be 5.57 kJ mol^{-1} and 7.04 as in Fig 5 and as mentioned in Table 1, a value within the range described in [32] (33-84 kJ mol^{-1}). While Table 2 shows enthalpy, entropy and Gibbs free energy which are the functions important to the limited stable phase of Al_2O_3 for two samples at the nanoscale, the positive sign of Gibbs is a reaction, not spontaneous i.e. the increasing of heat on samples due to an increase in entropy (exothermic reaction), this the function gives formation if endotherm or exothermic reaction but it doesn't have details any information about the reactions of speed.

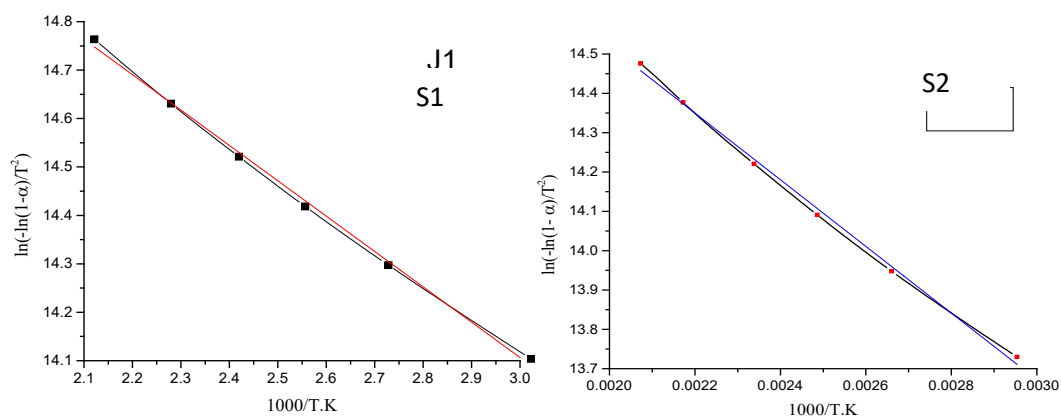


Fig. 4. Coast-Redfern plot for thermal degradation of two samples at the constant heating rate of $10^{\circ}\text{C}/\text{min}$.

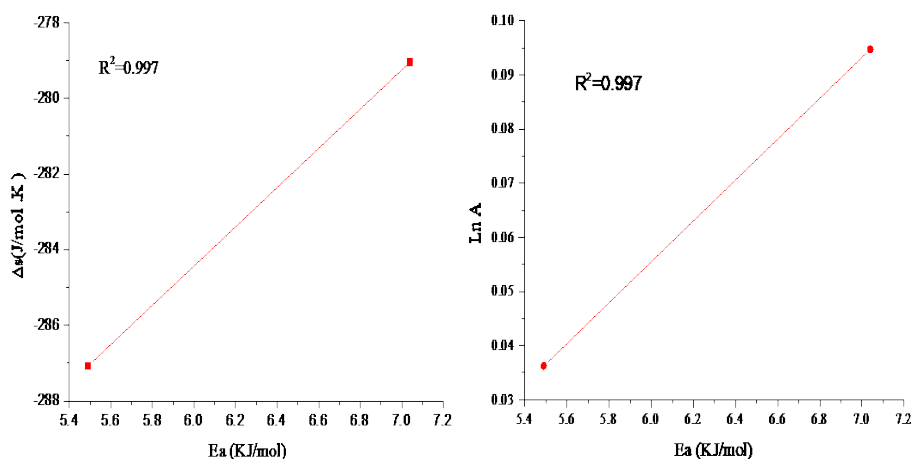


Fig. 5. Plot of activation energy versus $\ln A_0$ for the thermal decomposition of Al_2O_3 .

Table 1. Activation energy and relations associated with Gibbs function.

Sample	Activation Energy, E (KJ/mol)	Peak temperature, K	ΔH , KJ/mol	$-\Delta S$, J/mol	ΔG , KJ/mol
S1	5.49	573.391	0.72256	-0.2871	165.331
S2	7.04	583.576	2.18787	-0.279	165.032

Table 2. Shows reaction constant.

sample	peak temp. K	Activation energy Ea (kJ/mol)	reaction rate (S^{-1}) constant (A0)	R ²
S1	632.391	5.49	0.036222329	0.997
S2	629.576	7.04	0.094758978	0.997

5. Conclusion

Biofabrication of the α -Al₂O₃ nanoparticles was effectively created, and their properties were examined. The α -Al₂O₃ exhibits seven of the active modes of phonons for Raman modes at the Brillouin zone, it notes that several factors contribute to the electronic structure of Al₂O₃ at high temperatures, including the interaction between electrons and phonons and the expansion of the thermal lattice, the thermal properties proved that loss weight was fast and obtained the sable phase of oxide, one of the reasons of the bands emissions in samples is the defect levels obtaining of unsaturated bonds and the dangling bonds which existence on the nanostructure of surfaces that supports to form additional levels of energy in the crystals that have a broad bandgap. The thermal stability of Al₂O₃ (alumina) has been measured through thermogravimetric analysis (TGA) and heat flow measurements. The material remains structurally intact even at high temperatures, indicating that Al₂O₃ is a good thermal material for a variety of applications.

References

- [1] Gangwar J.; Kim J.; Kumar A.;Bhatnagar D.;Senthil K.; Tripathi,S. K.; Yong K.; Srivastava A. K., *Nanoscale*, 2015,7, 13313-13344; <https://doi.org/10.1039/C5NR02369F>
- [2] P. Kumar, B. K. Gupta, *RSC Advances*, 2015, 5, 24729; <https://doi.org/10.1039/C4RA15383A>
- [3] Gondoni P; Mazzolini P; Russo V.*Solar Energy Materials and Solar Cells*,2014,128,248-253. <https://doi.org/10.1016/j.solmat.2014.05.035>
- [4] He H., Orlando R., Blanco M. A., Pandey R., Amzallag E., Baraille I., Rérat M., *Physical Review. B*,2006, 74, 195123; <https://doi.org/10.1103/PhysRevB.74.195123>
- [5] S. S. Kumar; E. J. Rubio;M. Noor-A-Alam; G. Martinez;S. Manandhar; V. Shutthanandan, S. Thevuthasan ; C. V. Ramana, *J. Phys. Chem. C*, 2013, 117, 4194; <https://doi.org/10.1021/jp311300e>
- [6] R. Manigandan, K. Giribabu, S. Munusamy, S. P. Kumar,S. Muthamizh, T. Dhanasekaran, A. Padmanaban,R. Suresh, A. Stephen and V. Narayanan, *CrystEngComm*,2015, 17, 2886; <https://doi.org/10.1039/C4CE02390K>
- [7] K. K. Dey, A. Kumar, R. Shanker, A. Dhawan, M. Wan,R. R. Yadav and A. K. Srivastava, *RSC Adv.*, 2012, 2,1387; <https://doi.org/10.1039/C1RA00710F>
- [8] A. A. Balandin, *Nat. Mater.*, 2011, 10, 569; <https://doi.org/10.1038/nmat3064>
- [9] P. D. Shima and J. Philip, *Ind. Eng. Chem. Res.*, 2014, 53, 980; <https://doi.org/10.1021/ie403086g>
- [10] A. Puzder, A. J. Williamson, F. A. Reboredo and G. Galli, *Phys. Rev. Lett.*, 2003, 91, 157405; <https://doi.org/10.1103/PhysRevLett.91.157405>
- [11] D. Segev and S. H. Wei, *Phys. Rev. B: Condens. Matter*, 2005, 71, 125129; <https://doi.org/10.1103/PhysRevB.71.125129>
- [12] S. Takami, R. Hayakawa, Y. Wakayama and T. Chikyow, *Nanotechnology*, 2010, 21, 134009; <https://doi.org/10.1088/0957-4484/21/13/134009>
- [13] Al Ogaili, H.A.T., Abbas, S.I., Mohammed, M.A.*Chalcogenide Letters*, 2020, 17(5), pp. 251–255; https://chalcogen.ro/251_OgailiHAT.pdf
- [14] S. Farhadi, J. Safabakhsh and P. Zaringhadam, *J. Nanos truct. Chem.*, 2013, 3, 69; <https://doi.org/10.1186/2193-8865-3-69>
- [15] TrinklerL.; BerzinaB., JevsjutinaZ., GrabisJ. , SteinsI. , BailyC.J. Trinkler et al., *Optical Materials* 34 (2012) 1553-1557; <https://doi.org/10.1016/j.optmat.2012.03.029>
- [16] Abed FG, Jubeir NJ, Al Ogaili, HAT. *AIP Conference Proceedings.*, 2024, 2922(1), 040006; <https://doi.org/10.1063/5.0183132>

- [17] Saad KhalidRahi, RusulAdnan Al-Wardy, Hanan Abd Ali Thjeel Al Ogaili, Baghdad Science Journal 2024, 5(22) 3356-3367
- [18] V.A. Pustovarov, T.V. Perevalov, V.A. Gritsenko, T.P. Smirnova, A.P. Yelisseyev, Thin Solid Films, 519, 6319-6322 (2011); <https://doi.org/10.1016/j.tsf.2011.04.014>
- [19] C. Lin, M. Yu, Z. Cheng, C. Zhang, Q. Meng, J. Lin, Inorg. Chem., 47, 49-55(2008); <https://doi.org/10.1021/ic700652v>
- [20] D. Dasgupta, F. Demichelis, C.F. Pirri, A. Tagliaferro, Phys. Rev. B., 43,2131-2135 (1991); <https://doi.org/10.1103/PhysRevB.43.2131>
- [21] R. Hari Krishna, B.M. Nagabhushana, H. Nagabhushana, R.P.S. Chakradhar, N.Suriya Murthy, R. Sivaramakrishna, C. Shivakumara, J.L. Rao, T. Thomas, J. Alloys Comp., 589, 596-603 (2014); <https://doi.org/10.1016/j.jallcom.2013.11.221>
- [22] R. Hari Krishna, B.M. Nagabhushana, H. Nagabhushana, R.P.S. Chakradhar, R.Sivaramakrishna, C. Shivakumara, T. Thomas, J. Alloys Comp., 585, 129-137(2014); <https://doi.org/10.1016/j.jallcom.2013.09.037>
- [23] S. Wang, C. Zhang, G. Sun, Y. Yuan, L. Chen, X. Xiang, Q. Ding, B. Chen, Z. Li, X. Zu, J. Lumin., 2014,153, 393-400; <https://doi.org/10.1016/j.jlumin.2014.03.072>
- [24] B. Umesha, B. Eraiah, H. Nagabhushana, B.M. Nagabhushana, G. Nagaraja, C. Shivakumara, R.P.S. Chakradhar, J. Alloys Comp., 2011,509, 1146-1151; <https://doi.org/10.1016/j.jallcom.2010.09.143>
- [25] C. Hu, H. Liu, W. Dong, Y. Zhang, G. Bao, C. Lao, Z.L. Wang, Adv. Mater., 19,470-474 (2007); <https://doi.org/10.1002/adma.200601300>
- [26] Y. Zhang, K. Han, T. Cheng, Z. Fang, Inorg. Chem., 46, 4713-4717 (2007); <https://doi.org/10.1021/ic0701458>
- [27] Prashanth P.A.; Raveendr, R.S. ; Hari Krishn R.; Anand S.;Bhagya N.P.;Nagabhushan B.M.;Lingaraju K., Naik H. R., Journal of Asian Ceramic Societies,2015, 3, 345-351; <https://doi.org/10.1016/j.jascer.2015.07.001>
- [28] Cava S, Tebcherani SM, Souza IA, Pianaro SA, Paskocimas CA, Longo E, Varela JA (2007) . Material Chemistry and Physics, 2007 ,103(55):394-399; <https://doi.org/10.1016/j.matchemphys.2007.02.046>
- [29] Gangwar J, Gupta BK, Tripathi SK, Srivastav AK. Nanoscale ,2015 ,7,13313-13344; <https://doi.org/10.1039/C5NR02369F>
- [30] Pezzotti G, Zhua W Physical Chemistry Chemical Physics, 2015, 17:2608-2627; <https://doi.org/10.1039/C4CP04244A>
- [31] Al-Ogaili, H.A.T., Hathot, S.F.Digest Journal of Nanomaterials and Biostructures, 2023, 18(3), pp. 1017–1024;
- [32] Roger H. F., Journal of the American Ceramic Society-French,1990, 13 (3),471-489; <https://doi.org/10.1111/j.1151-2916.1990.tb06541.x>